Microforging technique for rapid, low-cost fabrication of lens array molds

Craig R. Forest,* Miguel A. Saez, and Ian W. Hunter

Department of Mechanical Engineering, BioInstrumentation Laboratory, Massachusetts Institute of Technology, 77 Massachusetts Avenue, Room 3-147, Cambridge, Massachusetts 02139, USA

*Corresponding author: cforest@alum.mit.edu

Received 4 September 2007; revised 11 October 2007; accepted 16 October 2007; posted 7 November 2007 (Doc. ID 87136); published 19 December 2007

Interest in micro-optical components for applications ranging from telecommunications to life sciences has driven the need for accessible, low-cost fabrication techniques. Many microlens fabrication processes are unsuitable for applications requiring 100% fill factor, apertures $\sim$1000 μm with high numerical aperture, and scalability to large areas (e.g., tens of centimeters to meters) with millions of lenses. We report on a flexible, low-cost mold fabrication technique that utilizes a combination of milling and microforging. The technique involves first performing a rough cut with a ball-end mill. Final shape and sag height are then achieved by pressing a sphere of equal diameter into the milled divot. Using this process, we have fabricated molds for rectangular arrays of 1–10,000 lenses with apertures of 25–1600 μm, sag heights of 3–130 μm, interlens spacings of 250–2000 μm, and fill factors up to 100%. Mold profiles have a roughness and figure error of 68 nm and 354 nm, respectively, for 100% fill factor, 1000 μm aperture lenses. The required forging force was modeled as a modified open-die forging process and experimentally verified to increase nearly linearly with surface area. The optical performance of lens arrays injection molded from microforged molds was characterized by imaging the point spread function and was found to be in the range of theoretical values. The process can be easily adapted to lenticular arrays as well. Limitations include milling machine range and accuracy. © 2007 Optical Society of America

OCIS codes: 220.4000, 120.4610, 120.6660, 120.6650.

1. Introduction

Miniaturization of devices and techniques to submillimeter scales holds much promise, including reducing cost, increasing portability and speed of analysis, and parallelism. Optical engineering must match these device sizes to continue to deliver, for example, sensitive, noninvasive, accurate measurement. Some instrumentation [1] requires arrays of thousands of tiny high numerical aperture (NA) lenses, tightly packed with 100% fill factor, ϕ (the ratio of the active refracting area to the total contiguous area occupied by the lens array), with apertures of 1000 μm and f number <5.

A wide variety of microlens array fabrication techniques currently exist ranging from lithographic techniques to diamond turning. Such techniques produce a mold master which can be cheaply replicated. Laser-based techniques are frequently discussed in the literature and involve the precise melting of a glass substrate [2] or photoresist [3] using a laser source. Photoresist reflow is a lithographic technique commonly used to fabricate microlens arrays by melting cylindrical photoresist posts onto the substrate [4]. Microlens arrays can also be produced directly in a homogeneous photosensitive glass using a photothermal process, which exposes the glass substrate to UV light through a mask [5]. The UV exposure and subsequent thermal development initiates the formation of a crystallized region, which constricts the soft undeveloped glass, forming a spherical shape due to surface tension. Chemical methods such as ion exchange have also been developed to produce planar microlens arrays with a parabolically distributed refraction index [6]. These planar arrays can be monolithically fabricated on a planar polymer or glass substrate by allowing a dopant to diffuse into the planar substrate through a mask. Another noteworthy technique is microjet printing, which involves

0003-6935/07/368668-06$15.00/0

jetting lens polymer onto a glass substrate and allowing it to solidify into a plano–convex lens [7].

These processes, with the exception of diamond turning, can often deliver exquisite replication of 15–500 μm aperture lenses that are often limited to square close-packed ($\phi = \pi/4 = 78\%$) or approaching hexagonally close packed ($\phi = 91\%$). Efforts to increase ϕ have not resulted in accurate lenses over the full aperture [4]. Achieving high NA can also be challenging, as typical lens' sags of this size are 1–20 μm. These processes can also be relatively expensive and time consuming to implement, and are limited in area that can be patterned to the diameter of a wafer, typically ~100–150 mm.

Diamond turning, for high machine and tooling costs, can produce microlens arrays with 250 nm figure error and 9 nm roughness over 1000 μm apertures and 100% fill factor, as well as a variety of other sizes. High costs can be distributed if the master is replicated, such as by injection molding. Limitations include the area that can be patterned, high startup costs, and fragile tooling. Sag height can be limiting as well, as the tools need to match the part slope over large distances (e.g., several millimeters).

In this work, we sought to develop a low-cost, flexible mold fabrication technique that could match the figure error of diamond turning. This novel method also employs readily available three-axis machining centers and minimizes processing steps.

2. Methods

A. Milling and Forging

Our milling and microforging process is shown schematically in Fig. 1, accompanied by photographs of a 100 lens mold and injection-molded lens array produced using this process. To fabricate the lens array molds, an aluminum substrate is first faced and polished. Next, a rough cut is performed with a ball-end mill. The final shape and sag height are then achieved by pressing a sphere of equal diameter into the milled divot. The reasoning behind the process is that the mill determines the majority of the mold figure, and subsequent forging with a ground, polished sphere (206 nm figure error, 19 nm roughness) imparts a near perfect figure and roughness to the mold without substantial deformation that could affect neighboring lenses in a tightly packed array. After mold fabrication, injection molding is performed. In practice, molds were created using titanium-nitride coated ball-end mills and tungsten-carbide spheres. A machining center (Haas, VF-OE) was used for lens mold fabrication. The system has 5.0 μm accuracy and 2.5 μm repeatability in all axes with work volume of 0.8 m $\times$ 0.4 m $\times$ 0.5 m. Experiments to determine the required forging force were performed using a 90 kN hydraulic press (Devin, LP-500).

B. Process Characterization

The quality of the lens molds produced with this technique was determined using two parameters: figure error and average roughness (Ra). These two parameters were calculated from mold surface profiles measured using a stylus profilometer (Mitutoyo, SV-3000) with a 2 μm radius tip, 1 μm lateral resolution, and 1 nm transverse resolution. From these raw data, we implemented several algorithms to measure figure error and surface roughness. Figure error was calculated over 80% aperture by comparing the measured surface profile to the desired shape. By shifting the desired shape relative to the measured profile, we find the optimal fit (least error) and compute their average absolute difference. For roughness, we first remove from the measurement low frequency information associated with the mold's round shape by successively fitting and subtracting the second, first, and zeroth order polynomials to measurement segments. The roughness is then calculated as the average Ra of this series of segments.

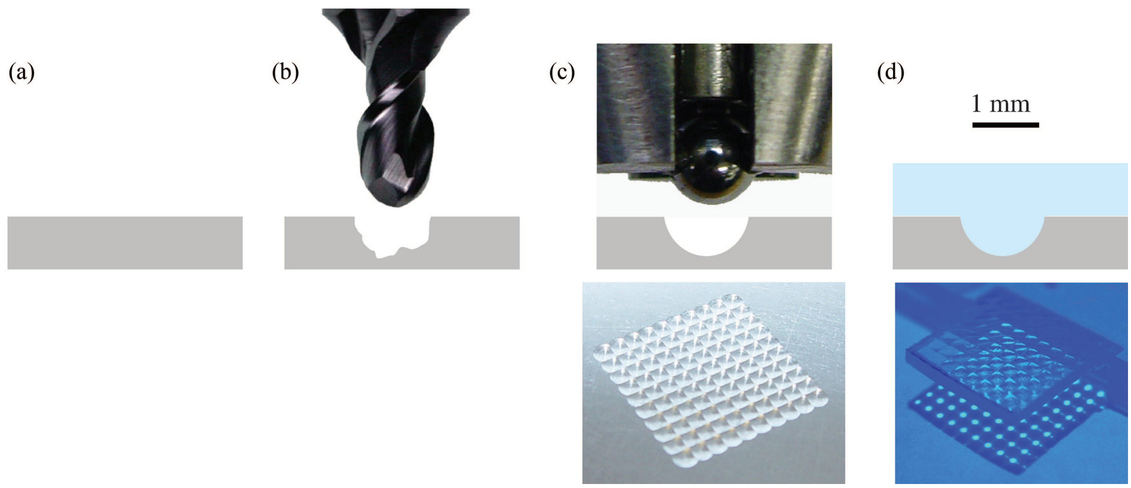

Fig. 1. (Color online) Schematic of the lens array mold manufacturing process and photographs of a 100 lens array mold and molded part. (a) Blank aluminum mold is faced and polished. (b) Rotating ball-end mill is used to cut an array of divots. (c) Tungsten-carbide sphere is lowered onto the surface to deform the divots to the final shape. (d) Mold is used to injection mold lens arrays.

C. Optical Characterization

The optical performance of the manufactured lens arrays was evaluated via measurements of their point spread function (PSF) using an optical apparatus based on a design by Lee *et al.* [8]. In this apparatus, a HeNe laser (Uniphase model 106-1) with output centered at 632.8 nm was spatially filtered and collimated. The radius of the collimated beam was truncated using an iris diaphragm and then further reduced by a telescope comprised of a pair of positive lenses. The lens array being tested was attached to a two-axis linear stage perpendicular to the incoming beam. Last, the resulting image was magnified by a 60× microscope objective mounted on a translational stage, and captured with a CCD (Photometrics, Cascade 650) having 653 × 492 pixels and a pixel size of 7.4 μm × 7.4 μm. Lens arrays produced using the combined milling and forging process, as well as forging alone were tested. A commercially available Spindler and Hoyer ground glass lens with a focal length of 5 mm was also tested for comparison. When imaging the PSF, the iris was adjusted such that the diameter of the incoming beam matched the lens aperture, and the lens array was aligned such that the beam was incident on only one of the lenses. The resulting image was focused by adjusting the distance between the microscope objective and the lens array.

3. Theory

A. Forging Model

As we seek to create spherical lens impressions in an aluminum mold, theoretical modeling of the required force was performed. We started with the open-die forging model by Kalpakjian and Schmid [9], given as

$$F_0 = Y_f \pi r^2\left(1 + \frac{2\mu r}{3h}\right) \tag{1}$$

for a cylindrical slug with radius r and height h where F_0 is the forging force, Y_f is the flow stress of the material (≈ true stress at 100% true strain), and μ is the coefficient of friction (≈0.2).

We then modified the model for hemispherical impressions on a planar substrate, assuming that the tool is much more stiff than the workpiece, to be

$$F = Y_f A_s\left(1 + \frac{\mu d}{3z}\right), \tag{2}$$

where A_s is the impression surface area, d is the lens aperture, and z is the forge depth. A_s and z, respectively, are given by

$$z(d,\ R) = R - \sqrt{R^2 - \frac{d^2}{2}}, \tag{3}$$

$$A_s(d,\ R) = 2\pi R^2\left(1 - \frac{\sqrt{R^2 - \dfrac{d^2}{2}}}{R}\right), \tag{4}$$

where R is the lens radius of curvature. In this modified model, the contact area between the tool and workpiece is that of a hemispherical impression rather than a slug's cylindrical cross section. The model predicts the required force, F, to create a spherical impression of depth, z, and aperture, d, for a range of mold materials, lens sizes, and sag heights.

B. Point Spread Function

The PSF describes the response of an optical system to an input point source and is often referred to as the impulse response function [10]. The degree of blurring and aberrations measured in the PSF relative to the theoretical, diffraction limited function is a measure of the quality of the optical system. The PSFs for convex lenses with circular and square apertures, respectively, are given by

$$I_c(x) = \left|2\,\frac{J_1\!\left(2\pi(\mathrm{NA})\dfrac{x^2}{\lambda}\right)}{2\pi(\mathrm{NA})\dfrac{x^2}{\lambda}}\right|^2, \tag{5}$$

$$I_{\mathrm{sq}}(x) = \left|2\,\frac{\sin\!\left(2\pi(\mathrm{NA})\dfrac{x^2}{\lambda}\right)}{2\pi(\mathrm{NA})\dfrac{x^2}{\lambda}}\right|^2, \tag{6}$$

where NA is the numerical aperture of the lens, λ is the wavelength, x is the spatial position on the screen, and J_1 is a Bessel function of the first kind [10]. Using a small angle approximation, NA is approximated by r/f, where r is the beam radius and f is the focal length. For a plano–convex lens, the focal length is given by

$$f = \frac{R}{n - 1}, \tag{7}$$

where R is the lens radius of curvature and n is the lens index of refraction. The PSFs for square or circular apertures are characterized by a bright central region, which physically limits the resolution of an image created by a lens. The size of this so-called Airy region for a square aperture convex lens is given by

$$d_{\mathrm{Airy}} = \frac{\lambda}{\mathrm{NA}}. \tag{8}$$

The region's diameter for a circular aperture can be found by multiplying by a factor of 1.22.

4. Results and Discussion

Using this process, we have fabricated molds for rectangular arrays of 1–10,000 spherical lenses with apertures of 250–1600 μm, sag heights of 3–130 μm,

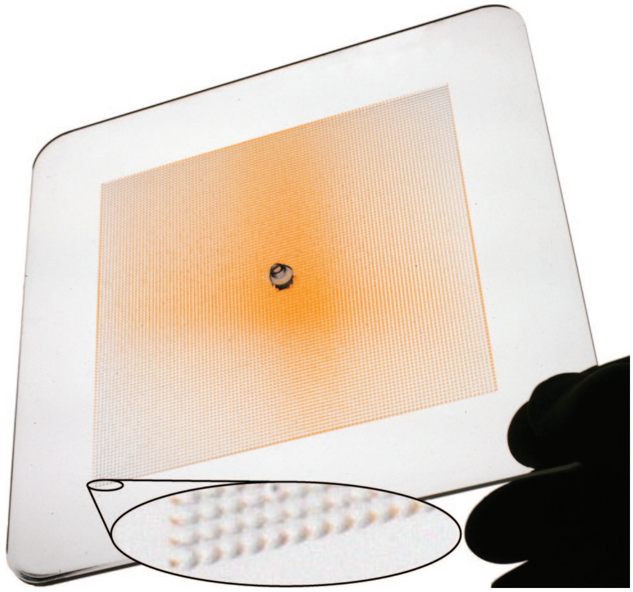

Fig. 2. (Color online) Photograph of a rectangular array of 10,000 lenses injection molded from a milled/microforged mold in PMMA. The spherical lenses each have a 1000 μm square aperture, 2.5 mm radius of curvature, 100 μm sag height, and 100% fill factor. The central feature, a sprue, is an artifact of the injection molding process.

interlens spacings of 250–2000 μm, and ϕ up to 100%. Images of a 100 lens array and its corresponding mold are shown in Fig. 1. A photograph of a 10,000 lens array is shown in Fig. 2.

A. Forging Force

Using a hydraulic press to form impressions in an aluminum 6061 substrate, we were able to compare our model with the experiment, as shown in Fig. 3. These experiments were conducted with several sphere diameters (10–25.4 mm). The results indicate that one can well predict the required forging force for typical lens sizes. For the smallest surface areas, the conservative model deviates from the experimental results by up to three times. Typical lenses with 1,410 μm aperture and 2.5 mm radius of curvature have a surface area of 1.6 mm^2 and require 1 kN of forging force. The machining center used for this work has a 25 kN forging force capability.

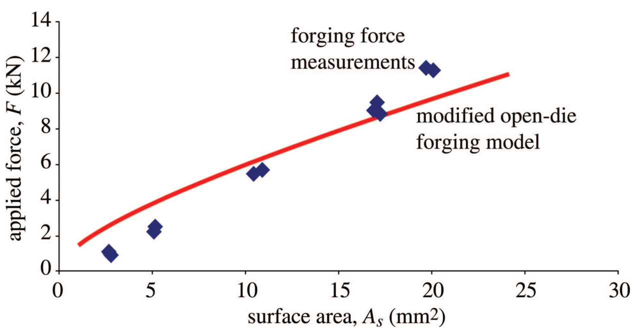

Fig. 3. (Color online) Forging force theory and experimental measurements versus molded surface area.

B. Figure Error and Roughness

Numerous molds were fabricated, measured, and analyzed as described. The results for the mold figure error and roughness are shown in Fig. 4. For lens array molds with $\phi \geq 80\%$, figure error decreases monotonically with increasing mill depth (decreasing forge depth). Since the forging process does not remove material but plastically deforms it, the neighboring lenses in tightly packed arrays are affected by the forging process. On the other hand, the roughness generally increases (degrades) with increased mill depth. This can be attributed to the milling tool's roughness, which is much larger than the sphere's 19 nm roughness. For fill factors less than 80% forging alone has a superior combination of figure error and roughness.

The advantage of the combined process is clear when comparing the figure error and roughness of the lens mold to that created by either process alone. Purely milled divots typically have 1700 nm figure error and 300 nm roughness (not shown), independently of ϕ. Purely forged divots have figure error that is dependent on ϕ (See Fig. 4 left, at worse 1800 nm for $\phi = 100\%$ and roughness of 31 nm independent of ϕ. The optimal combination results in a figure error that is 4–5 times better than either process alone, while roughness remains good at ~68 nm. For 100% fill factor lens array molds, milling to the full depth and subsequently forging to the full depth results in the best figure with reasonable roughness.

We also measured the figure error and roughness of the corresponding injection-molded parts. For molds with $\phi = 100\%$ made using the optimum combination of milling and forging, measurements of injection-molded lens arrays showed that figure error increased from 354 to 939 nm relative to the mold, while roughness decreased from 68 to 36 nm. This is reasonable given the 1%–2% linear shrinkage of polymethylmethacrylate (PMMA) upon cooling after molding, and corresponding attenuation of high frequency features.

We also fabricated $\phi = 100\%$ lens array molds with 250–1000 μm apertures and constant radius of curvature of 2.5 mm. Roughness of the molds was independent of lens aperture, averaging 75 nm. Figure error of the molds improved as lens aperture was reduced: 1000 μm aperture, 50.5 μm sag lenses had 350 nm figure error (see Fig. 4 left); 500 μm aperture, 12.5 μm sag lenses had 150 nm figure error; and 250 μm aperture, 3.1 μm sag lenses had 110 nm figure error. Smaller apertures are prohibited by the accuracy of the machining center and end mill tool.

Drawbacks include required calibration of the depth of milling and forging tools, which has an inherent uncertainty of 1 μm. Thermal expansion of the machining center can affect lens sag. In addition, elastic "springback," upon unloading the forge can contribute to sag errors. All combined, we measured these factors to affect sag by, at most, 20 μm. Lenses with large surface areas (e.g., >57 mm^2 each), may exceed typical machining center force capabilities.

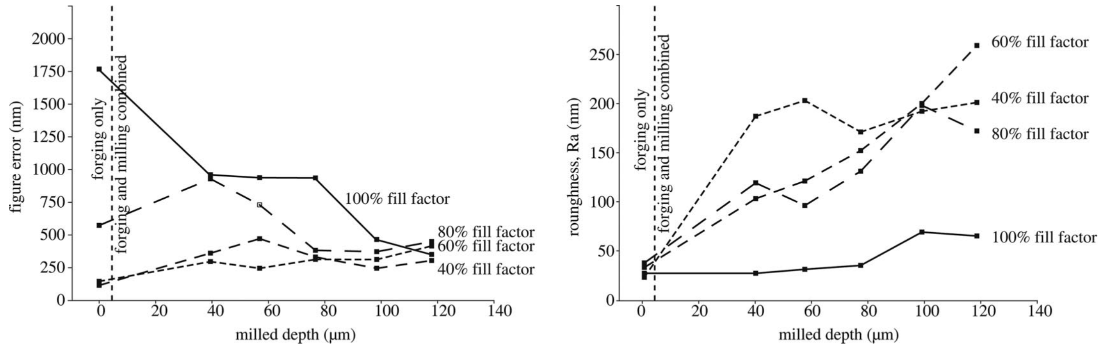

Fig. 4. Figure error (left) and roughness (right) of lens array molds. All lenses have 120 μm total sag height, so increasing milled depth implies that a larger percentage of the final figure was determined by milling. (left) As milled depth increases, the figure error generally improves while the roughness increases (degrades) somewhat to a plateau, but is still small.

C. Optical Performance

The PSFs measured with injection molded lens arrays fabricated using forging only and the combined milling and forging process were measured using the optical measurement apparatus as described. A ground glass lens was also tested for comparison. The ground glass lens produced the sharpest PSF with the bright center region clearly defined. With the exception of a few scattered bright lobes near the center, the forged lens also produced a well defined Airy region. The lenses fabricated using the combined milling and forging process produced PSFs with brighter, more scattered fringes. Despite this, the bright central region was easily identifiable.

In addition to a qualitative evaluation of the PSF images, Airy region sizes were measured and compared to their expected values from Eqs. (5) and (6) to determine lens quality, as shown in Fig. 5, with $R = 2.5$ mm and $n = 1.49$ for PMMA. Theoretical Airy region sizes for round and square lenses with focal length 5 mm are 8.2 ± 2.1 μm and 6.8 ± 1.7 μm, respectively. The uncertainty in the region size arises from the measurement of the input beam's diameter. The resolution of this measurement is 250 μm.

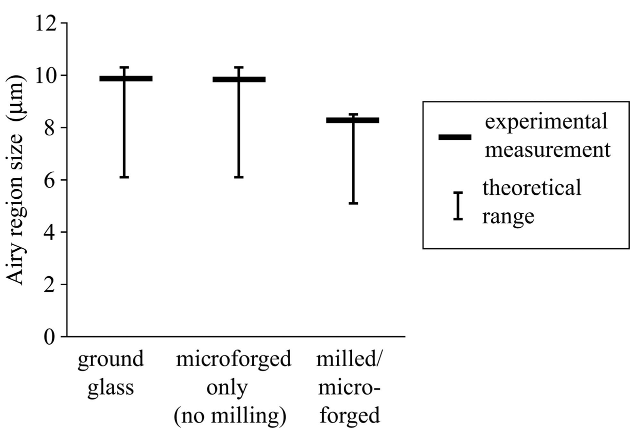

Fig. 5. Theoretical and experimental Airy region sizes for the tested lenses. The glass and forged lenses have round apertures, while the microforged and milled lens arrays have square apertures ($\phi = 100\%$).

5. Conclusions

A novel fabrication technique for microlens array molds has been described, which relies on a combination of milling and microforging. Relative to diamond turning, this process is much cheaper and simpler to implement while delivering a comparable figure error and roughness within an order of magnitude.

A theoretical model for the forging process has been developed and verified experimentally. Various lens array molds, as well as their respective PMMA injection-molded parts, were fabricated, measured, and analyzed in order to determine the process range and the optimal process parameters experimentally. For lens arrays with $\phi \geq 80\%$, the combination of milling and microforging offers great potential for the fabrication of molds with low figure error and roughness. For such tightly packed lens arrays varying in lens aperture from 250–1000 μm, we have demonstrated that figure error will be $\leq$354 nm and roughness will be $\sim$75 nm. We have used this process to mold lens arrays containing more than 10,000 lens elements, over a 102 mm $\times$ 104 mm area. Should lens arrays with $\phi < 80\%$ be desired, forging alone can provide superior figure errors of $<$250 nm and roughness of 31 nm.

The PSFs of the manufactured lenses were imaged in order to evaluate their optical performance. Based on measurements of the PSF, forging alone offered the best performance, comparable to that of ground glass lens. Lenses fabricated using the combined milling and forging technique performed within the theoretical range. Lens arrays injection molded from microforged molds have been demonstrated to have the required optical performance for sensitive optical detection. Thus, this flexible, low-cost, scalable process could supplant many other lens array manufacturing processes that operate within this size and density range.

We gratefully acknowledge the generous support of the National Science Foundation, Sandia National Laboratories, the Massachusetts Institute of Technology (MIT) BioInstrumentation Laboratory, and the MIT Undergraduate Research Opportunities Program.

References

1. S. Morgenthaler and W. G. Thilly, "Summed multi-allelic risk: logical and statistical models for discovery of carrier genes in human populations," Mutat. Res. **615,** 28–56 (2007).
2. M. Fritze, M. B. Stern, and P. W. Wyatt, "Laser-fabricated glass microlens arrays," Opt. Lett. **23,** 141–143 (1998).
3. T. R. Jay and M. B. Stern, "Preshaping photoresist for refractive microlens fabrication," Opt. Eng. **33,** 3552–3555 (1994).
4. H. Yang, C.-K. Chao, M.-K. Wei, and C.-P. Lin, "High fill-factor microlens array mold insert fabrication using a thermal reflow process," J. Micromec. Microeng. **14,** 1197–1204 (2004).
5. N. F. Borelli and D. K. Morse, "Microlens array produced by a photolytic technique," Appl. Opt. **27,** 476–479 (1988).
6. M. Oikawa, K. Iga, S. Misawa, and Y. Kokubun, "Improved distributed-index planar microlens and its application to 2-D lightwave components," Appl. Opt. **22,** 441–442 (1983).
7. D. L. MacFarlane, V. Narayan, J. A. Tatum, W. R. Cox, T. Chen, and D. J. Hayes, "Microjet fabrication of microlens arrays," IEEE Photon. Technol. Lett. **9,** 1112–1114 (1994).
8. Y.-C. Lee, C.-M. Chen, and C.-Y. Wu, "Spherical and aspheric microlenses fabricated by excimer laser LIGA-like process," J. Manuf. Sci. Eng. **129,** 126–134 (2007).
9. S. Kalpakjian and S. Schmid, *Manufacturing Engineering and Technology* (Academic, 2001).
10. E. Hecht, *Optics* (Academic, 2001).